IEEE Access
Multidisciplinary | Rapid Review | Open Access Journal

SPECIAL SECTION ON DATA-DRIVEN MONITORING, FAULT DIAGNOSIS AND CONTROL OF CYBER-PHYSICAL SYSTEMS

Received December 23, 2017, accepted January 20, 2018, date of publication January 31, 2018, date of current version March 15, 2018.

Digital Object Identifier 10.1109/ACCESS.2018.2800158

Tunable Surface-Plasmon-Polariton Filter Constructed By Corrugated Metallic Line and High Permittivity Material

JIANG LUO[1], (Student Member, IEEE), JIN HE[1], (Senior Member, IEEE), ALIT APRIYANA[2], GUANGYIN FENG[2], (Member, IEEE), QIJUN HUANG[1], AND YUE PING ZHANG[2], (Fellow, IEEE)
[1]School of Physics and Technology, Wuhan University, Wuhan 430072, China
[2]School of Electrical and Electronic Engineering, Nanyang Technological University, Singapore 639798

Corresponding author: Jin He (jin.he@whu.edu.cn)

This work was supported in part by the National Natural Science Fundamental of China under Grant 61774113, Grant 61574102, and Grant 61404094, in part by the Fundamental Research Funds for the Central Universities, Wuhan University, under Grant 2042017gf0052 and Grant 2042014kf0238, and in part by the China Post-Doctoral Science Foundation under Grant 2012T50688.

ABSTRACT This paper presents the development of a novel surface plasmon polariton band-stop filter with tunable operating frequency. The tuning is done by embedding a high permittivity BST dielectric block into the gap of SPP transmission line (T-line). An obvious transmission dip at the certain frequency is observed due to Fabry-Pérot interference. The notch frequency is sensitive to the variation of the dielectric constant of the BST ceramic. Specifically, a transmission dip up to −11.5 dB is observed at the notch frequency of 8.12 GHz when the dielectric constant of BST is 425; the notch frequency shifts from 8.7 to 7.6 GHz when the dielectric constant of BST increases from 375 to 475. To further verify the functions of the proposed SPP filter, a prototype is fabricated on the Rogers-4003 dielectric substrate. The measured and the simulated results show good agreements. The proposed structure has outstanding features of a very compact area, simple fabrication, and tunable operating frequency, which have great potential for the applications in tunable frequency selection metamaterials devices.

INDEX TERMS Surface plasmon polariton (SPP), high permittivity, BST, destructive interference, band-stop filter.

I. INTRODUCTION

Surface plasmon polariton (SPP), which propagates at the interface between dielectric and metal at optical frequency, has attracted a lot of attentions because of its potential in applications in optical communication, sensing, sub- wavelength resolution imaging, and so on [1]–[6]. However, metallic materials usually behave as good conductors at lower frequency region such as microwave and terahertz frequencies, thus showing weak confinement to electromagnetic waves. Therefore, a so-called spoof SPP (SSPP) structure, which has geometry of engineered hole-array in metallic plate, has been proposed based on plasmonic metamaterial mechanism [7]. Since the plasma frequency of SSPP structure depends on the geometric parameters, its dispersion curve and operating frequency band are designable.

Some schemes have been proposed to realize the effective excitation of SPP wave at microwave and terahertz frequencies, such as, the hole-array or grating on metallic films, and grooving on metallic lines techniques [8]–[11]. Recently, a 2-D SPP structure that has periodically grooved metallic strip on a thin dielectric film was developed [12]. With the conversion from guided wave mode to SPP mode, high efficiency and low loss transmission line (T-line) was achieved [13]. Moreover, some passive SPP devices, such as waveguide, resonator, filter and frequency selection device, were successfully designed [14]–[17]. Due to its sub-wavelength feature size, SPP based devices can achieve the targeted performance within compact area. In past decades, SPP devices usually only had fixed operating frequency points or narrow bands, which limited their applications in frequency tunable devices. Recently, some SPP devices have been developed towards dynamic functionalities such as modulating, tuning and manipulating electromagnetic (EM) waves at microwave and terahertz regimes. Various techniques have been proposed to achieve the dynamic functionalities, such as tuning the dispersion of SPP waves by the concepts of coding and programmable metasurfaces [18], the phase control of dual fundamental Gaussian beams [19], the guiding-out coupling structures [20], the dielectric-thickness adjusting method [21], anisotropic metamaterials [22], etc. Some tunable or controllable SPP devices have thus been realized accordingly. However, SPP filters that can continuously tune SPP propagation over a broadband frequency have rarely been reported.

In this work, a high-permittivity dielectric material is embedded into the SPP T-line structure to control the propagation behavior of SPP wave [23]. Over a wide frequency pass-band region, the SPP T-line exhibits high transmission efficiency. On the other hand, at the designed stop-band, the transmission is significantly declined due to the high reflection introduced by the high-permittivity dielectric material. Simultaneously, the operating frequency band can be tunable because of the temperature or applied field dependent dielectric constant of the BST dielectric material [24]. Compared with the existing SPP filters, the proposed structure achieves a band-stop filter with tunable operating frequency in compact area. The new mechanism raised here can promote the research and application of frequency tunable SPP devices and also some tunable frequency selection metamaterials or metasurfaces.

II. TUNABLE SPP FILTER DESIGN

The schematic diagram of the proposed SPP filter (denoted as SPP-F) with BST dielectric material is plotted in Fig. 1. The SPP propagation at 6 GHz and 8.12 GHz are shown in Fig. 1 (b) and Fig. 1 (c), respectively. The former demonstrates high transmission, while the later shows transmission dip at 8.12 GHz. The SPP-F was designed using a copper film (thickness of 0.017 mm) with a whole area of 222.5×69.7 mm^2, which was fabricated on a Rogers-4003 dielectric substrate with relative permittivity of 3.55, loss tangent of 0.0027, and thickness of 0.508 mm. As can be seen, the SPP-F is mainly composed of a periodically grooved metallic strip, mode converters, and a high-permittivity dielectric block.

In order to improve transmission efficiency, it is important to achieve wideband impedance matching and momentum matching. A mode converter featured as a smooth bridge between the coplanar waveguide (CPW) with 50 ohms impedance and SPP T-line is designed. It converts TEM wave to TM wave with a gradual increasing of gradient depth of grooves from 0 to 3.0 mm [13]. Specifically, the CPW with 50 ohms impedance is realized with the length and width of single conducting track as 13.0 mm and 9.0 mm, respectively. The gap between a pair of return conductors and the central track of the CPW is eventually optimized to be 0.36 mm. The dimensions of the SPP unit cell are $p = 4.5$ mm, $a = 1.5$ mm, and $b = 3.0$ mm, denoting the period, width, and length of grooves, respectively. The BST dielectric block (red block in Fig. 1 (a)) is MgO doped high-permittivity $(BaxSr1\text{-}x)TiO_3$ ceramic material with the dielectric constant optimized around 425 and loss tangent factor of 0.01.

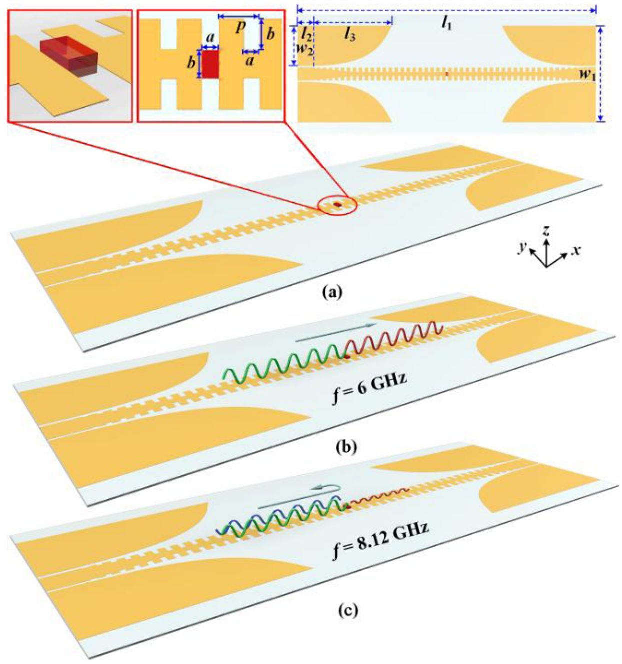

FIGURE 1. (a) The proposed SPP-F, in which the red part is a high-permittivity dielectric block, embedding into a through-hole with the size of $3.0 \times 1.5 \times 0.2$ mm^3 on the substrate and contacting both the sides of copper layer, the yellow part is a layer of copper and the gray part is a dielectric substrate layer of Rogers-4003, and all optimized geometric parameters are $l_1 = 222.5$ mm, $l_2 = 13.0$ mm, $l_3 = 58.5$ mm, $w_1 = 69.72$ mm, $w_2 = 30.0$ mm, $p = 4.5$ mm, $a = 1.5$ mm, $b = 3.0$ mm. (b) SPP propagation at 6 GHz with high transmission. (c) SPP propagation at the notch frequency of 8.12 GHz.

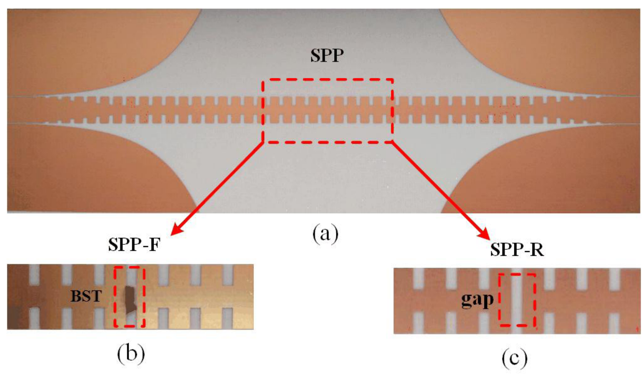

FIGURE 2. The photograph of the fabricated samples (a) SPP T-line. (b) SPP-F T-line (only the different areas are presented, the rest is the same as the SSP T-line). (c) SPP-R T-line (only the different areas are presented, the rest is the same as the SSP T-line).

The width and length of the dielectric block are $a = 1.5$ mm and $b = 3.0$ mm, respectively, whereas the thickness of the dielectric block is 0.4 mm. At the same time, a rectangular hole is constructed on the dielectric substrate at the center of SPP-F with a size of $3.0 \times 1.5 \times 0.2$ mm^3.

Note that the dielectric block is embedded into the rectangular hole, which is electrically in touch with both sides of the SPP T-line. For validations, the three samples including SPP, SPP-F and SPP-R are fabricated, measured and analyzed.

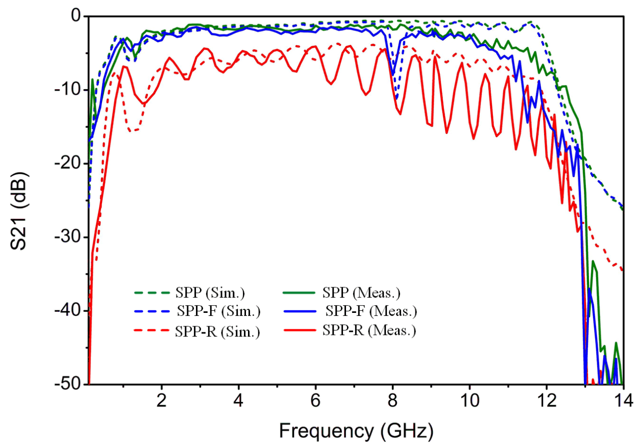

FIGURE 3. **The simulated and measured transmission coefficient S21 for SPP, SPP-F and SPP-R.**

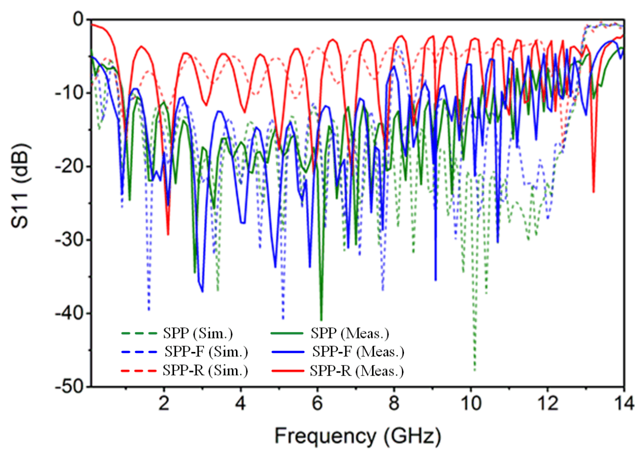

FIGURE 4. **The simulated and measured reflection coefficient S11 or S22 for SPP, SPP-F and SPP-R.**

Note that SPP-R is the same structure as SPP-F without the high-permittivity dielectric block. The photographs of the fabricated samples including SPP-F, SPP, and SPP-R are shown in Fig. 2.

III. EXPERIMENTAL RESULTS AND ANALYSIS

A. S-PARAMETERS

The simulated and measured S-parameters (transmission coefficient S21 and reflection coefficient S11 or S22) results are plotted in Fig. 3 and Fig. 4. It can be seen that the measured results are in good agreement with the simulated results when the operating frequency is less than 10 GHz. However, the measurement results deviate from the simulation results when the operating frequency is higher than 10 GHz. It is mainly due to the SMA connector (SMA KFD20 HD 16-9) used only supporting a maximum operating frequency of 12 GHz. As a consequence, the transmission efficiency is seriously degraded when approaching the limiting operating frequency of the SMA connector.

It can be seen in Fig. 3 and Fig. 4 that the SPP T-line achieves a simulated S21 of less than −1.5 dB and a S11 of better than −10 dB over the bandwidth of 2-10 GHz, respectively; while the measured S21 is less than −3 dB and S11 is also better than −10 dB at the operating frequency range from 2 GHz to 10 GHz. The slight difference between measured and simulated results may mainly be resulted from the matching error and metal loss. In contrast, due to strong reflection loss, the simulated and measured S21 and S11 of the SPP-R from 0.1 GHz to 12 GHz are worse than −5 dB and −10 dB, respectively. Besides, the S-parameter curves exhibit obvious ripples over the observed frequency band. After embedding the BST block, the transmission performance of the T-line is significantly improved. As shown in Fig. 3, the simulated S21 of SPP-F has a good agreement with intact SPP T-line at the frequency range from 0.1 GHz to 7.8 GHz and 9 GHz to 12 GHz, while the simulated S11 of SPP-F is better than −10 dB apart from the high-permittivity-modulated frequency band of 7.8-8.8 GHz. Moreover, a simulated transmission dip with a value up to −11.5 dB is observed at the notch operating frequency of 8.12 GHz. Thus, the SPP-F exhibits a characteristic of band-stop. The 3-dB bandwidth is 0.35 GHz from 7.945 GHz to 8.295 GHz, and the relative bandwidth is around 4.3%. From the experimental results, it can be seen that the measured S21 of SPP-F has a good agreement with SPP T-line at the operating frequency range from 0.1 GHz to 7.5 GHz and 8.4 GHz to 10 GHz. The measured S11 of SPP-F is better than 10 dB apart from the high-permittivity-modulated frequency band of 7.6-8.3 GHz and the high frequency band of more than 10 GHz. The obvious transmission dip appear at the notch frequency of 8 GHz. The measured 3-dB bandwidth is 0. 36 GHz from 7.82 GHz to 8.18 GHz, while the relative bandwidth is 4.5 %. It is noted that the notch frequency is observed at 8 GHz in experiment, deviating from the simulated result at 8.12 GHz, which is mainly due to the fabrication error and dielectric loss, especially for the BST dielectric block, because the dielectric constant of BST ceramic is sensitive to temperature and applied electric field. The above measured results suggest that the band-stop SPP filter can be tuned at the desired operating band by the high-permittivity dielectric material BST block.

B. THE NEAR ELECTRIC-FIELD DISTRIBUTION

The electric filed distribution of the aforementioned structures are simulated to gain deeper physical insight into the effect of dielectric block on the SPP wave propagation. Two operating frequency points are selected and analyzed, one is 6 GHz with high transmission, while the other one is 8.12 GHz at the transmission dip. Fig. 5 presents the simulated results of near electric-field distribution (the Ez component) for the SPP, SPP-F and SPP-R at 6 GHz on an observation z plane that is 2 mm above the structure. It is clearly observed that the mode converter from CPW to SPP T-line is of high efficiency and the signal energy can propagate excellently at the SPP and SPP-F. Moreover, the electric filed distribution exhibits remarkable field confinement

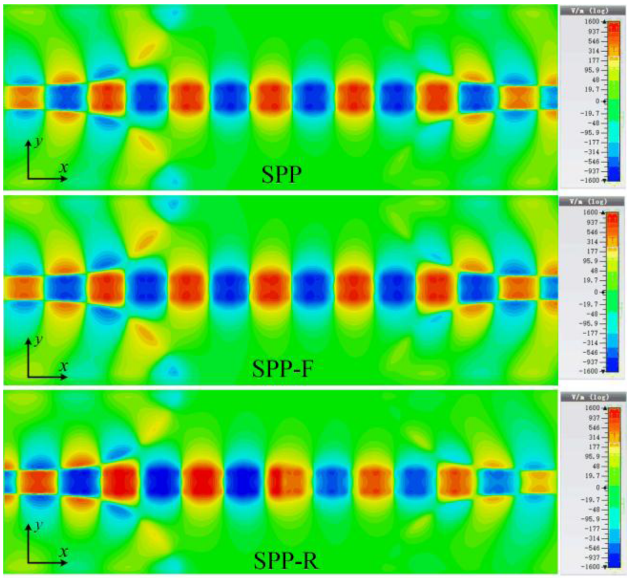

FIGURE 5. The near electric-field distribution for the SPP, SPP-F and SPP-R at the operating frequency of 6 GHz.

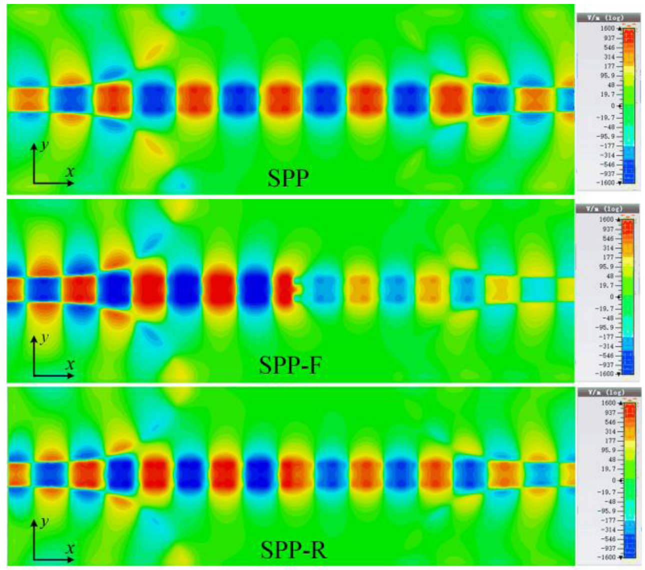

FIGURE 6. The near electric-field distribution for the SPP, SPP-F and SPP-R at the operating frequency of 8.12 GHz.

characteristic. As a comparison, the transmitted electric field for SPP-R weakens to a large extent due to the reflection loss at the gap, which is consistent with the transmission degrade shown in Fig. 3. The corresponding near electric-field distributions at the operating frequency of 8.12 GHz are presented in Fig. 6. As can be seen, the near-field distribution images of SPP and SPP-R are similar with those observed at 6 GHz. However, the near electric-field distribution of SPP-F differs a lot for SPP-F at 6 GHz, showing that the energy is strongly reflected by the dielectric block, which is in accordance with the transmission dip observed in Fig. 3. Thus, we can draw a conclusion that the gap in the SPP T-line will result in a high reflection loss, and if the gap is bridged by a high-permittivity dielectric block, the composed SPP T-line would show a high transmission efficiency as good as intact SPP T-line except for the notch frequency.

C. THE PRINCIPLE FOR BAND-STOP FILTERING

Then, we will reveal the underlying physical mechanism according to the interface momentum-matching analysis. SPP wave is the collective oscillations of electrons excited in the dielectric-metal interface and propagates along the interface. The dispersion relation of SPP wave can be described by

$$k_x = \frac{\omega}{c}\left(\frac{\varepsilon_1 \varepsilon_2}{\varepsilon_1 + \varepsilon_2}\right)^{1/2} \tag{1}$$

Where, k_x is the wave vector component in the x direction, ω is the angular frequency, c is the velocity of light in vacuum, while ε_1 and ε_2 are the permittivity (or effective permittivity) of dielectric material and metallic layer, respectively. Fig. 7 shows the dispersion relation curves of SPP structure and vacuum (light line), which are simulated using Eigen mode in CST Microwave Studio. As can be seen, the dispersion curve of SPP significantly deviates from the

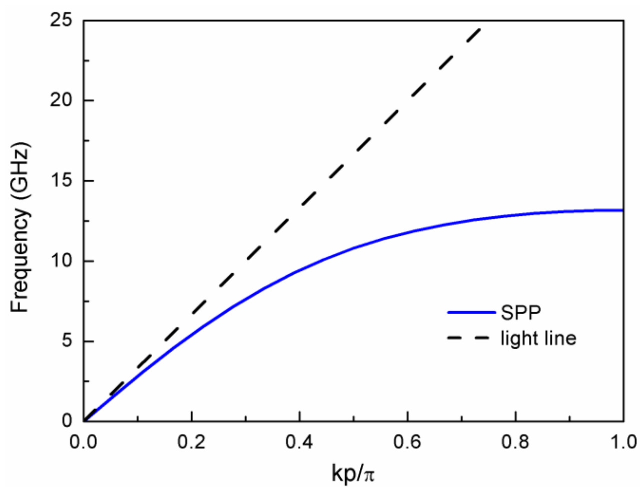

FIGURE 7. The dispersion curves of SPP structure and light line.

light line as the frequency increases and exhibits the feature of slow wave effect. The cutoff frequency of the proposed structure in this work is around 12 GHz. For frequencies below the cutoff frequency, the field can be tightly confined in the interface between air and metallic strip and the SPP wave propagates along the interface with a high efficiency. However, for the T-line with an air gap, the momentum matching is not satisfied in the gap, which will lead to a high reflection. Thus, the transmission efficiency of SPP-R is much lower than that of SPP. Moreover, ripples observed on S21 curve in Fig. 3 can be attributed by the interference of the transmitted signal and the reflected signal by the gap. When a high-permittivity dielectric block is embedded into the gap, SPP-F exhibits a high transmission efficiency. The BST block works as a dielectric waveguide bridging the left and right side of SPP T-line. However, at the notch frequency, the main transmission signal and the multi-reflection signal interfere destructively due to the Fabry-Pérot interference, which results in a transmission dip. The notch frequency depends on the dielectric constant of the block since the phase difference is related to the dielectric constant. The relationship between phase and dielectric constant can be described by

$$\Delta\varphi = \frac{2\pi}{\lambda} \cdot 2d = \frac{4\pi d}{\lambda_0} \cdot \sqrt{\varepsilon_{eff}} \quad (2)$$

Where $\Delta\varphi$ is the phase difference between the main transmission signal and the multi-reflection signal, λ and λ_0 are wavelength in medium and vacuum, d is the thickness of dielectric block, and ε_{eff} is the effective dielectric constant (SPP wave propagates in an effective medium composed by a substrate, dielectric block, and air) [25]. When the phase difference of these waves satisfies $\Delta\varphi = (2n + 1) \cdot \pi$ (n is an integer), these anti-phase waves cancel out each other. Then, a transmission dip will appear at a certain operating frequency. Here we observe the destructive interference with n = 0. Because of the remarkable transmission dip, the SPP-F T-line can also works as a SPP band-stop filter. It is also noted that the other transmission dip can also be observed at a higher frequency of 28.5 GHz, which can be ascribed to the mode of n = 1. Theoretically, the 1st order mode will be located at 24.36 GHz, while the frequency blue-shift is mainly due to the decrease of BST dielectric constant at high frequencies.

In Eq. (2), the theoretical ε_{eff} for destructive interference condition is calculated as 37.9. Then, we estimate the dielectric constant of the effective medium using the linear superposition of dielectric substrate, BST block and air in the gap region. The thickness of air layer in z axis is selected as 1 mm, then the energy of SPP waves at the boundary reduces to 1/10 of the strength close to the surface of SPP T-line. According to the dielectric constants and volume ratio of three matters, $\varepsilon_{\mathrm{eff}}$ can be estimated as 35.5, which agrees well with the theoretical value. Thus, the physical mechanism raised here is convincing.

It is worth noting that the dielectric constant of BST is sensitive to the temperature or applied electric field. BST is a kind of ferroelectric, which can achieve very high permittivity due to the spontaneous polarization. The increase in temperature will induce ferroelectric-paraelectric phase transition and applied electric field will lead to the reorientation of dipole moment, both of which will cause the change of dielectric constant. For $Ba_xSr_{1-x}TiO_3$, the transition temperature (Curie temperature, T_C) can be expressed as [26]

$$T_c(x) = 42 + 439.37x - 95.95x^2 \quad (3)$$

When $x = 0.5$, T_C is 237 K. And thus, with the increasing of temperature (usually above T_C), the dielectric constant can be described by

$$\varepsilon(T) = \frac{C}{T - T_c} \quad (4)$$

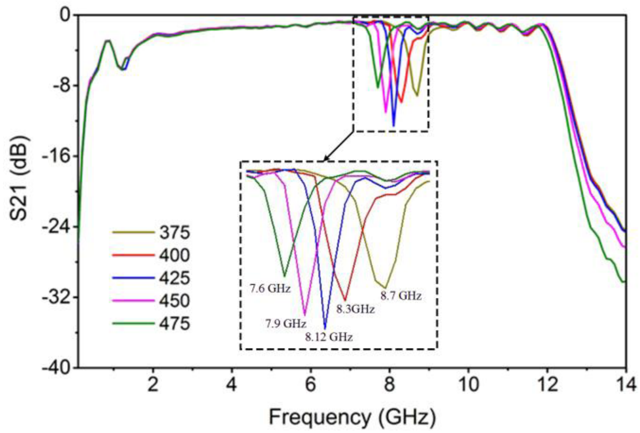

FIGURE 8. **The transmission coefficient of SPP-F under different BST dielectric constants.**

Where C is the Curie constant, which is in the order of 10^5 K for BST. If an electric field is applied, the dielectric can be tuned over a large range. The tuning range can be written by [26]

$$\frac{\varepsilon(0) - \varepsilon(E)}{\varepsilon 0} \approx 2\beta\varepsilon^2(0)\varepsilon_0^3 E \quad (5)$$

Where $\varepsilon(0)$ and $\varepsilon(E)$ represent the dielectric constant without electric field and under electric field E, respectively, β is the third-order nonlinear polarization coefficient, and ε_0 is the vacuum permittivity.

As previously reported [27], the dielectric constant of pure BST film is about 1750 at zero bias at 10 GHz, and the tunable range reaches 59% under a field of 60 kV/cm. For MgO doped BST, the dielectric constant will decrease, however a relatively high tunability is retained. As an example, 60wt% MgO doped $Ba_{0.55}Sr_{0.45}TiO_3$ ($\varepsilon_r = 99.8$) possesses a tuning range of 18.4% under a bias of 6 V/μm.

As described above, the temperature and applied electric field affect the dielectric constant of the BST block, resulting in a wide tunable characteristic. Thus, the frequency tunable characteristic of the SPP-F is also investigated. The dielectric constant of BST block is defined between 375 and 475 with a step size of 25. The transmission coefficient under various dielectric constants are presented in Fig. 8. It can be found that the transmission dip frequency shifts to a lower frequency as the dielectric constant of BST block increases. The notch frequency decreases from 8.7 GHz to 7.6 GHz, and the average frequency shift for the one-unit-permittivity increase is 11 MHz when the dielectric constant increases from 375 to 475. It can be explained by Eq. (2) that increased dielectric constant will result in an increased wavelength. Then as for identical phase difference, the notch frequency of the SPP-F will be shifted to a lower frequency. Hence, SPP reflection-type filter with tunable operating frequency can be achieved which can modulate SPP wave over a broad frequency band.

IV. CONCLUSION

In summary, the SPP T-line with a high-permittivity BST dielectric block embedded was found in this paper to be effective in controlling the propagation behavior of SPP wave. A novel SPP band-stop filter with tunable operating frequency has been achieved within compact area. It is both numerically and experimentally shown that the transmission performance of SPP-F is as good as the intact SPP T-line at the broadband frequency. Furthermore, an obvious transmission dip is observed at the notch frequency of 8.12 GHz, which can be attributed by the high reflection induced by Fabry-Pérot interference. It is worth noting that the notch frequency of transmission dip depends on the dielectric constant of BST block. Specifically, the notch frequency shifts from 8.7 GHz to 7.6 GHz when the dielectric constant increases from 375 to 475. Hence, this SPP modulation effect will promote its application into frequency tunable SPP devices and also some tunable frequency selection metamaterials or metasurfaces.

V. METHODS

The simulation of the SPP-F, SPP, and SPP-R structures were performed using the commercial software, CST Microwave Studio. The transmission coefficient and reflection coefficient of these structures were simulated at the broadband operating frequency range from 0.1 GHz to 14 GHz. The experimental samples were fabricated using Rogers-4003 dielectric substrate with relative permittivity of 3.55, loss tangent of 0.0027, and thickness of 0.508 mm. The BST dielectric block is MgO doped high-permittivity (BaxSr1-x)TiO_3 ceramic material that was prepared by ceramic sintering method. The S-parameters (transmission coefficient S21 and reflection coefficient S11 or S22) of the fabricated samples were measured using N5247A PNA-X Microwave Network Analyzer.

REFERENCES

[1] S. A. Maiser, *Plasmonics: Fundamentals and Applications*. New York, NY, USA: Springer, 2007.

[2] W. L. Barnes, A. Dereux, and T. W. Ebbesen, "Surface plasmon subwavelength optics," *Nature*, vol. 424, no. 6950, pp. 824–830, 2003.

[3] E. Ozbay, "Plasmonics: Merging photonics and electronics at nanoscale dimensions," *Science*, vol. 311, no. 5758, pp. 189–193, Jan. 2006.

[4] H. Yao and S. Zhong, "High-mode spoof SPP of periodic metal grooves for ultra-sensitive terahertz sensing," *Opt. Express*, vol. 22, no. 21, pp. 25149–25160, 2014.

[5] N. Fang, H. Lee, C. Sun, and X. Zhang, "Sub-diffraction-limited optical imaging with a silver superlens," *Science*, vol. 308, pp. 534–537, Apr. 2005.

[6] S. Kawata, Y. Inouye, and P. Verma, "Plasmonics for near-field nano-imaging and superlensing," *Nature Photon.*, vol. 3, pp. 388–394, Jul. 2009.

[7] J. B. Pendry, L. Martín-Moreno, and F. J. Garcia-Vidal, "Mimicking surface plasmons with structured surfaces," *Science*, vol. 305, pp. 847–848, Aug. 2004.

[8] A. P. Hibbins, B. R. Evans, and J. R. Sambles, "Experimental verification of designer surface plasmons," *Science*, vol. 308, no. 5722, pp. 670–672, Apr. 2005.

[9] C. R. Williams, S. R. Andrews, S. A. Maier, A. I. Fernández-Domínguez, L. Martín-Moreno, and F. J. García-Vidal, "Highly confined guiding of terahertz surface plasmon polaritons on structured metal surfaces," *Nature Photon.*, vol. 2, pp. 175–179, Mar. 2008.

[10] G. Li *et al.*, "Terahertz coherent control of surface plasmon polariton propagation in subwavelength metallic hole arrays," *Appl. Phys. Lett.*, vol. 100, no. 19, 2012, Art. no. 191115.

[11] S. A. Maier, S. R. Andrews, L. Martín-Moreno, and F. J. García-Vidal, "Terahertz surface plasmon-polariton propagation and focusing on periodically corrugated metal wires," *Phys. Rev. Lett.*, vol. 97, pp. 176805-1–176805-4, Oct. 2006.

[12] X. Shen, T. J. Cui, D. F. Martin-Cano, and J. Garcia-Vidal, "Conformal surface plasmons propagating on ultrathin and flexible films," *Proc. Nat. Acad. Sci. USA*, vol. 110, no. 1, pp. 40–45, Jan. 2013.

[13] H. F. Ma, X. Shen, Q. Cheng, W. X. Jiang, and T. J. Cui, "Broadband and high-efficiency conversion from guided waves to spoof surface plasmon polaritons," *Laser Photon. Rev.*, vol. 8, no. 1, pp. 146–151, 2014.

[14] T. Zhang *et al.*, "Integrated optical gyroscope using active Long-range surface plasmon-polariton waveguide resonator," *Sci. Rep.*, vol. 4, Jan. 2014, Art. no. 3855.

[15] X. Shen and T. J. Cui, "Planar plasmonic metamaterial on a thin film with nearly zero thickness," *Appl. Phys. Lett.*, vol. 102, no. 21, 2013, Art. no. 211909.

[16] Q. Zhang, H. C. Zhang, J. Y. Yin, B. C. Pan, and T. J. Cui, "A series of compact rejection filters based on the interaction between spoof SPPs and CSRRs," *Sci. Rep.*, vol. 6, Jun. 2016, Art. no. 28256.

[17] J. Y. Yin, J. Ren, H. C. Zhang, B. C. Pan, and T. J. Cui, "Broadband frequency-selective spoof surface plasmon polaritons on ultrathin metallic structure," *Sci. Rep.*, vol. 5, Feb. 2015, Art. no. 8165.

[18] H. C. Zhang, T. J. Cui, J. Xu, W. Tang, and J. F. Liu, "Real-time controls of designer surface plasmon polaritons using programmable plasmonic metamaterial," *Adv. Mater. Technol.*, vol. 2, no. 1, 2017, Art. no. 1600202.

[19] C.-F. Kuo and S.-C. Chu, "Launching of surface plasmon polaritons with tunable directions and intensity ratios by phase control of dual fundamental Gaussian beams," *Opt. Exp.*, vol. 25, no. 9, pp. 10456–10463, 2017.

[20] J. Duan *et al.*, "High-efficiency chirality-modulated spoof surface plasmon meta-coupler," *Sci. Rep.*, vol. 6, May 2017, Art. no. 1354.

[21] H. Zhuang, F. Kong, K. Li, and Y. Wang, "A dielectric-thickness-adjusting method for manipulating graphene surface plasmon polariton," *Plasmonics*, vol. 12, no. 3, pp. 605–610, 2017.

[22] Z. Shao *et al.*, "Manipulating surface plasmon polaritons with infinitely anisotropic metamaterials," *Opt. Express*, vol. 25, no. 9, pp. 10515–10526, 2017.

[23] X. Fu *et al.*, "Mode jumping of split-ring resonator metamaterials controlled by high-permittivity BST and incident electric fields," *Sci. Rep.*, vol. 6, Aug. 2016, Art. no. 31274.

[24] X. Wang, R. Huang, Y. Zhao, H. Zhou, and Z. Jia, "Dielectric and tunable properties of Zr doped BST ceramics prepared by spark plasma sintering," *J. Alloys Compound*, vol. 533, pp. 25–28, Aug. 2012.

[25] D. S. Bulgarevich, M. Watanabe, and M. Shiwa, "Aperture array Fabry–Pérot interference filter," *Opt. Commun.*, vol. 285, pp. 4861–4865, Nov. 2012.

[26] A. K. Tagantsev, V. O. Sherman, K. F. Astafiev, J. Venkatesh, and N. Setter, "Ferroelectric materials for microwave tunable applications," *J. Electroceram.*, vol. 11, pp. 5–65, Sep. 2003.

[27] J. H. Leach *et al.*, "Large dielectric tuning and microwave phase shift at low electric field in epitaxial $Ba_{0.5}Sr_{0.5}TiO_3$ on $SrTiO_3$," *J. Appl. Phys.*, vol. 107, no. 8, p. 084511, 2010.

JIANG LUO (S'15) was born in Jiangxi, China. He received the B.E. degree in electronic information engineering from Luojia College, Wuhan University, Wuhan, China, in 2013, where he is currently pursuing the Ph.D. degree at the School of Physics and Technology. His research interests include mm-wave/terahertz integrated circuits and systems, and metamaterials devices for wireless and optical communication applications.

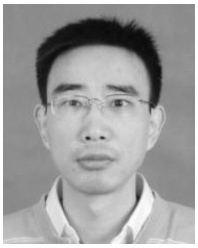

JIN HE (S'09–M'10–SM'12) received the Ph.D. degree from Nanyang Technological University, Singapore, in 2011. He was involved with analog/RF/mm-wave in both academia and industry in China and Singapore, respectively, from 2003 to 2013, holding positions as an Engineer, a Research Associate, a Senior Research Engineer, a Scientist, and a Project Leader. He joined Wuhan University, Wuhan, China, in 2013, where he is currently an Associate Professor with the School of Physics and Technology. His current research interests include analog/RF/mm-wave/THz integrated circuit design in CMOS/BiCMOS/SiGe for optical and wireless applications. He has served as a Technical Reviewer for the IEEE Transactions on Microwave and Theory Techniques, the IEEE Transactions on Electron Devices, IEEE Microwave and Wireless Components Letters, the *Electronics and Telecommunications Research Institute Journal*, and the *Journal of Electronic Science and Technology*.

ALIT APRIYANA received the B.E. degree in electrical and electronic engineering and M. Phil. degree in RF and telecommunication engineering from Nanyang Technological University, Singapore, in 2003 and 2004, respectively, where he is currently pursuing the Ph.D. degree. From 2004 to 2009, he was with EPCOS Pte Ltd, Singapore, as the Senior Engineer in RF surface acoustic wave filter design. In 2007, he was appointed the Design Leader of the GSM Group, EPCOS Pte Ltd. His research interests include analog/RF/millimetre-wave IC design and system architectures for wireless communications.

GUANGYIN FENG (S'12–M'16) received the B.E. degree from Northeastern University, Shenyang, China, in 2010, and the Ph.D. degree from Nanyang Technological University, Singapore, in 2016. Since 2016, he has been with Nanyang Technological University as a Research Fellow. His research interests include mm-wave/terahertz integrated circuits and systems for imaging and wireless communications.

QIJUN HUANG was born in Guangxi, China, in 1965. He received the B.S. degree in semiconductor physics and Ph.D. degree in microelectronics and solid-state electronics from Wuhan University, Wuhan, China, in 1986 and 2010, respectively. He is currently a Professor with Wuhan University. His current research interests include the design of analog and digital integrated circuits, embedded systems, and measuring instruments.

YUE PING ZHANG (M'03–SM'07–F'10) is currently a Full Professor of electronic engineering with the School of Electrical and Electronic Engineering, Nanyang Technological University, Singapore. He was a member of the Field Award Committee of the IEEE AP-S from 2015 to 2017, an Associate Editor of the IEEE Transactions on Antennas and Propagation from 2010 to 2016, and the Chair of the IEEE Singapore MTT/AP Joint Chapter in 2012. He has authored or co-authored numerous papers, including two invited papers in the Proceedings of the IEEE and one invited paper in the IEEE Transactions on Antennas and Propagation. He holds seven U.S. patents. He has made pioneering and significant contributions to the development of the antenna-in-package technology that has been widely adopted by chip makers for millimeter-wave applications. His current research interests include the development of antenna-on-chip technology and characterization of chip-scale propagation channels at terahertz for wireless chip area network. He is a Distinguished Lecturer of the IEEE Antennas and Propagation Society (IEEE AP-S). He was a recipient of the Best Paper Award from the Second IEEE/IET International Symposium on Communication Systems, Networks and Digital Signal Processing, in 2000, Bournemouth, U.K., the Best Paper Prize from the Third IEEE International Workshop on Antenna Technology, in 2007, Cambridge, U.K., and the Best Paper Award from the Tenth IEEE Global Symposium on Millimeter-Waves, in 2017, Hong Kong. He was the recipient of the prestigious IEEE AP-S Sergei A. Schelkunoff Prize Paper Award in 2012. He was selected by the Recruitment Program of Global Experts of China as a Qianren Scholar at Shanghai Jiao Tong University in 2012. He was the recipient of a William Meng Visiting Fellowship in 2005 and was appointed as a Visiting Professor by The University of Hong Kong in 2014.